Cyclotron resonance of electron inversion layers in Si (001) metal-oxide-semiconductor field-effect transistors (MOSFET's)

R. J. Wagner, T. A. Kennedy, and B. D. McCombe
Naval Research Laboratory, Washington, D.C. 20375

D. C. Tsui
Bell Laboratories, Murray Hill, New Jersey 07974

(Received 31 December 1979)

Cyclotron-resonance experiments on inversion-layer electrons in a series of large gate area Si metal-oxide-semiconductor field-effect transistors (MOSFET's) have been performed with a submillimeter laser system in conjunction with high-field Bitter-type magnets. The parameters determined from fits to the experimental magnetotransmission data, cyclotron effective mass and scattering time, have been studied as functions of laser wavelength, resonant magnetic field, inversion-layer density, temperature, and depletion charge. Results exhibit consistent and systematic behavior from sample to sample as functions of these various parameters. There are two distinct regions of density with different physical behavior. In both the high-density (metallic) and low-density (localized) regimes the experimental results appear to be influenced largely by electron-electron interactions. A transition region between these two extremes also exhibits distinctive behavior. These results are compared with other work, and possible explanations are discussed.

I. INTRODUCTION

Since the initial observations of cyclotron resonance (CR) of electrons in inversion layers on Si (001),[1] there have been many further optical and transport studies elucidating various properties of space charge layers in semiconductors.[2] The parameters determined by a cyclotron-resonance experiment, cyclotron effective mass and scattering time, have *not* been found to be simply related to the corresponding bulk semiconductor parameters. Unexpected dependences on carrier density,[3-5] magnetic field (frequency),[4-6] temperature,[7] and uniaxial stress[8,9] have been observed. As is usually suggested, these results, obtained on "real" systems, *may* provide insight concerning single-particle and many-body aspects of the "ideal" quasi-two-dimensional electron gas (2DEG). However, a good deal of caution must be exercised in the evaluation and interpretation of such data. For example, it has been shown recently[10] that the cyclotron effective mass determined from Shubnikov–de Haas experiments on Si (001) inversion layers may depend strongly on the presence of Na^+ ions at the Si-SiO_2 interface. Effects such as this may have played unintended roles in other 2DEG experiments and thus contributed to disagreements among experimental results obtained in different laboratories.

The device structure, a Si metal-oxide-semiconductor field-effect transistor (MOSFET), which is the experimental vehicle for the studies to be discussed, is shown pictorially in Fig. 1. The device is fabricated on a p-type substrate and has a conducting n-type channel which results from application of a positive voltage V_G between the metal gate and an Ohmic substrate contact. In equilibrium, the electric field developed across the thin SiO_2 insulator terminates at negative charge in the Si, i.e., the valence and conduction bands are bent downward. Initially, the charge is due to ionized acceptors in a depletion layer near the interface. When the bands are bent far enough, however, a conducting channel of mobile electrons (the inversion layer) is formed in a narrow region at the Si-SiO_2 interface. Due to the confining potential, motion of these electrons perpendicular to the interface is quantized into a series of electric field subbands while motion in the plane is unaffected. A schematic representation of the effective potential and the subbands for electrons on Si (001) is shown in Fig. 2. The conduction band of bulk Si consists of six equivalent minima located at 0.85 of the distance to the Brillouin-zone boundary along the ⟨100⟩ directions. The energy surfaces in momentum space projected onto the (001) plane are also shown in Fig. 2(a). Due to the electric field the two sets of valleys become inequivalent. The valleys with the heaviest mass perpendicular to the interface ($0.98m_e$) give rise to a set of subbands (unprimed) which lie lowest in energy [Fig. 2(b)]. These subbands are twofold degenerate (fourfold with spin). The other set of valleys with a light mass perpendicular to the interface ($0.19m_e$) give rise to a higher-lying set of subbands (primed). These subbands are fourfold degenerate (eightfold with spin). The energy separations between adjacent subbands and between the two sets of subbands depend sensitively on both the depletion charge

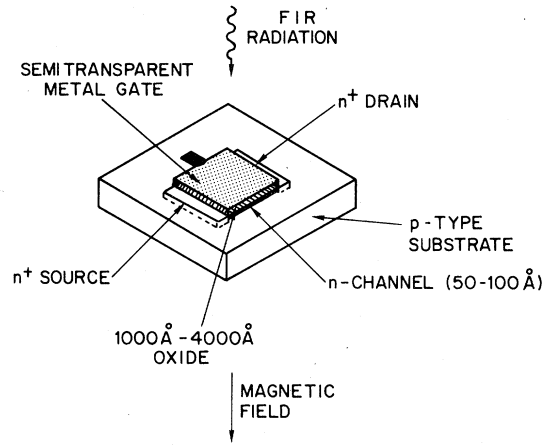

FIG. 1. Sketch of the large-area MOSFET used in these cyclotron-resonance experiments.

and the inversion charge.

In the following sections we describe detailed resonant magnetotransmission studies of a series of Si (001) MOSFET's over a range of electron densities, resonant magnetic fields, temperatures, and values of depletion charge. Section II presents information concerning device preparation and characteristics and experimental techniques used in the present studies. The experimental results are presented in Sec. III along with the data reduction procedures which were used to deduce cyclotron effective mass and scattering time from the data. The discussion of these results, Sec. IV, is organized along lines suggested by dc conductivity experiments. At high electron densities, inversion-layer conductivity appears to be nearly temperature independent as in a metal. On the other hand, at low densities, the conductivity is thermally activated, as expected

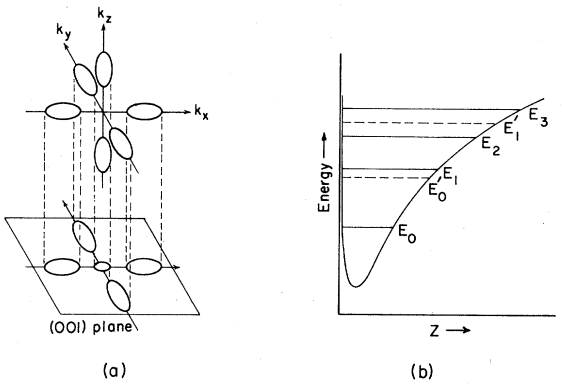

FIG. 2. (a) Si conduction-band structure as projected onto the (001) plane (interface). (b) Sketch of the electric field quantized levels for the twofold degenerate valleys (E_0, E_1, E_2, E_3) and fourfold degenerate valleys (E_0', E_1').

for transport in disordered systems. While this division for the optical experiments is somewhat arbitrary, the variation of the CR parameters does indicate some correlation with these limiting behaviors. In both cases, the CR results will be discussed with reference to previous experiments and theoretical calculations. The concluding section, Sec. V, summarizes and reemphasizes the results of this experiment. Suggestions as to possible lines for future work are made where there are areas of ambiguity or disagreement.

II. EXPERIMENTAL ASPECTS

The MOSFET's used in this experiment had a common geometry, shown in Fig. 1. These large-area devices (2.5×2.5 mm^2 gate area) were fabricated on (001) surfaces of 10–15 Ω cm p-type Si. Although a variety of processing steps were used, the highest quality (highest electron mobility, lowest fixed oxide charge) interfaces were grown by dry O_2 oxidation at 1100 °C followed by an anneal in Ar at 1100 °C and in H_2 at 380 °C. The gate was a semitransparent layer (~50 Å) of Ti. Source and drain contacts were phosphorous-diffused n^+-doped regions. The resulting devices, prepared at different times over a period of three years and under slightly different conditions, showed substantial variations in transport properties. The surface electron density n_s was determined from the gate voltage on the device through $n_s = (C_0/e)(V_G - V_T)$, where C_0 is the oxide capacitance per unit area and V_T is the threshold voltage for inversion layer (channel) formation at 77 K. Both the threshold and the density-voltage relationship agree with those determined from the Shubnikov–de Haas oscillations at 4.2 K. The effective electron mobility was determined from the zero-field channel conductance versus gate voltage at 4.2 K and the relationship $\sigma = n_s e \mu$. These results are shown in Fig. 3. A peak in the effective mobility is observed in all devices. It should be noted that at sufficiently low electron densities the conductivity is thermally activated in all samples, and the concept of an effective mobility becomes questionable. The density below which thermally activated conductivity is observed at 4.2 K is indicated by the arrow on the curves. It is clear from this figure that the value of the maximum effective mobility and the density at which it occurs varies from sample to sample; the density at which the maximum occurred moves systematically to lower values of n_s as the corresponding mobility increases.

The magnetic field dependence of the transmission of the inversion-layer electrons in the large-area MOSFET's was measured at different

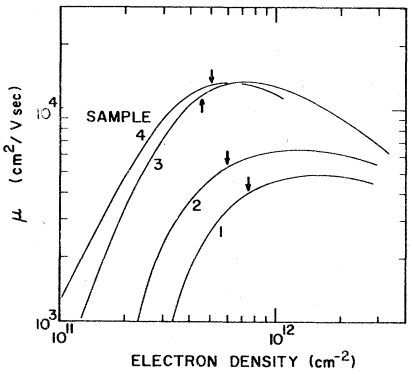

FIG. 3. Variation of effective mobility with density for the four samples studied in this experiment. The arrows indicate the densities below which the conductivity is thermally activated and above which the conductivity is metallic.

frequencies with a pulsed, optically pumped far-infrared (FIR) laser spectrometer.[11] By switching the MOSFET gate on and off coherently with alternate laser pulses, two signals, corresponding to a finite inversion-layer density and zero inversion-layer density, respectively, were derived from a single detector. These two signals were preamplified, separately boxcar integrated, and then divided in a ratiometer to give a dc signal proportional to the transmittance of the inversion layer at a density fixed by the square-wave voltage applied between the gate and the shorted source, drain, and substrate contacts (see Fig. 4). Since the method uses a single detector and ratiometry, it is a very effective means of eliminating noise from laser instabilities and other sources; it enables the observation of changes in transmission of less than 1% with good signal-to-noise ratio

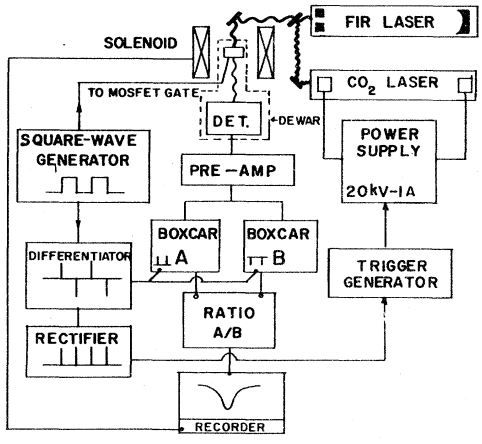

FIG. 4. Magneto-optical spectrometer used in the cyclotron-resonance experiments. The electronic arrangement allows the use of only one radiation detector.

for many laser lines. The laser pulse duration was about 50 μsec and the square wave on the gate was 100 Hz, i.e., gate on (or off) for 5 msec. The laser pulse was timed so as to probe the inversion layer about 1 msec after the gate voltage was cycled. Based on RC-time-constant considerations, it was concluded that the device had achieved equilibrium conditions prior to the laser probe over the density and temperature regions discussed in this paper. This was confirmed by the good agreement at all densities between the experimentally determined cyclotron-resonance line strength and that obtained from theoretical model calculations which will be discussed later.

The formation of an equilibrium depletion layer in low-temperature Si inversion-layer experiments has been widely discussed in the past few years with regard to its effect on electric subband splittings and apparent discrepancies in subband energies obtained at different laboratories.[12-14] Establishing equilibrium is particularly difficult at low temperatures for metal-oxide-semiconductor (MOS) capacitors where there are *no* source or drain contacts which can supply minority carriers, and it has also been shown that even for devices with source and drain contacts a full depletion layer is *not* established for long periods of time (hours) when the sample is cooled to helium temperatures under flat band or accumulation conditions in the dark.[12-14] A full depletion layer can be established at low temperatures in several ways: (1) cooling from liquid-nitrogen temperature or above under inversion conditions, (2) applying a positive gate voltage and band-gap light for a short time at low temperatures, and (3) applying a positive gate voltage while the sample is exposed to background radiation. In case (3) the negatively charged acceptors which form the fixed depletion charge are generated by photoionization of the neutral acceptors by the background infrared radiation with the free holes swept out by the applied voltage.

Although under the usual low-temperature conditions and at the electron densities studied, the present experiments involve only population of the lowest electric field subband [E_0 of Fig. 2(b)] and transitions among electrons within that subband (i.e., the cyclotron-resonance spectrum) could be affected by the relative separation between subbands. For example, a substantially increased cyclotron mass has been observed at low densities and high temperatures[7] and under uniaxial stress.[8,9] Under these conditions the upper heavy-mass subband [E_0' of Fig. 2(b)] may be nearly degenerate with the light-mass subband [E_0 of Fig. 2(b)]. In the present case room-temperature radiation was incident on the device during the experiment. This allowed

the establishment of a depletion layer close to the equilibrium depletion layer for strong inversion. Once established, changes in gate voltage above threshold have negligible effect on the depletion layer thickness and the resulting depletion charge density.[15] The effect of the depletion layer on the cyclotron resonance was investigated in some detail by illuminating the device with varying intensities of band-gap radiation. The results of these experiments are described in Sec. III.

It has been observed that distortions of CR line shape and position can occur in the typical plane-parallel (Fabry-Perot-type) device geometry.[16,17] Such effects were eliminated for the most part in these studies by either wedging the substrate itself or gluing an Si wedge to the device. Additional distortions caused by circular polarization of the beam by the light-pipe system at the longest wavelengths[17] were eliminated by placing a wire-grid linear polarizer immediately before the sample. Finally, a metallic aperture of roughly the gate area was placed in front of the sample in order to avoid light leakage. Such radiation, coherent with but phase shifted with respect to light traversing the active region of the device, could recombine with the transmitted radiation at the detector to create the appearance of anomalous field-dependent changes in "transmission."[17] At the lowest laser frequencies any residual (small) polarization problems were removed by averaging field sweeps in both the positive and negative direction.

At all wavelengths, the laser peak power was kept below 1 mW in order to avoid carrier heating. This is equivalent to a maximum high-frequency electric field of less than 0.01 V/cm. The magnetic fields used in these experiments were provided by a $2\frac{1}{2}$-in.-bore Bitter solenoid of the Naval Research Laboratory High Magnetic Field Facility.

III. EXPERIMENTAL RESULTS

Typical magnetotransmission spectra taken at 4.5 K on sample 3 are shown in Fig. 5 for three FIR frequencies and an inversion-layer density of 7.71×10^{11} cm^{-2}. The FIR frequencies are stated in terms of inverse wavelength $\tilde{\nu} = \omega/2\pi c$, where ω is the laser angular frequency. Two different procedures have been adopted to fit the data so as to extract the most reliable values of effective mass m^* and scattering time τ. Since these alternate approaches have been described elsewhere,[4,17] only a brief description will be included here. In both cases, the radiation is assumed to be incident on a classical, 2DEG at the Si-SiO_2 interface in the presence of a uniform static magnetic field B. (A quantum-mechanical treatment of the cyclotron resonance of a 2DEG has been given by Ando[18] and more recently by others.[19,20] Ando's results for a line broadened by short-range scattering centers exhibit quantum oscillations in the dynamical conductivity σ_{xx} as a function of magnetic field and a width proportional to $B^{1/2}$. The quantum oscillations are a result of the singular density of states of the 2DEG in a magnetic field modulating the absorption as the Landau levels are swept through the Fermi energy. For energies near $\hbar\omega_c$, the self-energy shift is very small. A more general treatment[19] has demonstrated that self-energy corrections vanish near $\omega = \omega_c$ for any type of scattering. Thus we expect that, except for the small quantum oscillation modulation, a classical model should give good results for the line shape and peak position when the possibility of field-dependent broadening is taken into account.)

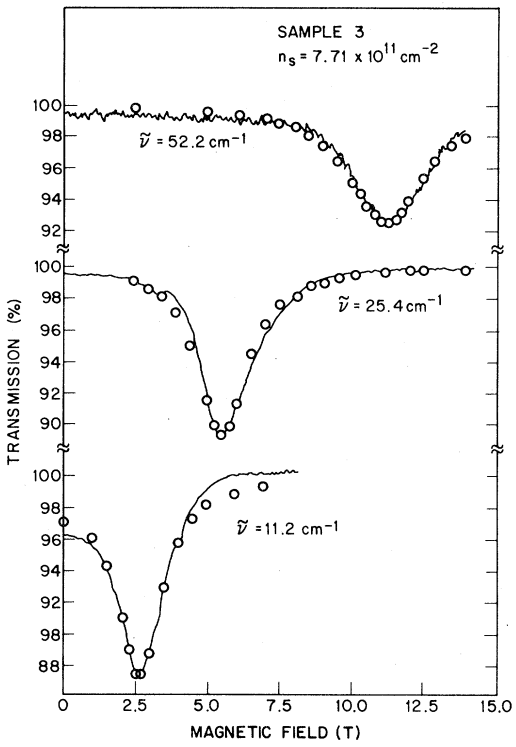

FIG. 5. Cyclotron-resonance transmission for sample 3 at three laser frequencies. The circles are line-shape fits obtained with Eq. (1). The fitting parameters are the following: at 52.2 cm^{-1}, $m^*/m_e = 0.201$, $\tau(B_c) = 7.5 \times 10^{-13}$ sec; at 25.4 cm^{-1}, $m^*/m_e = 0.203$, $\tau(B_c) = 13.6 \times 10^{-13}$ sec; and at 11.2 cm^{-1}, $m^*/m_e = 0.220$ and $\tau_0 = 14.9 \times 10^{-13}$ sec.

In the simpler case, multiple passes of radiation through the Si slab are neglected; i.e., the wedged slab is assumed to eliminate interference effects completely and the Si substrate is assumed to be semi-infinite. The resulting transmission

for linearly polarized radiation, when normalized to the gate-off, $n_s = 0$, condition, is

$$t = \frac{1}{2}\left(\frac{X^+}{X^+ + \omega_{ps}\tau(\omega_{ps}\tau+2)} + \frac{X^-}{X^- + \omega_{ps}\tau(\omega_{ps}\tau+2)}\right), \quad (1)$$

where $X^\pm = (\omega \pm \omega_c)^2\tau^2 + 1$, $\omega_{ps} = (4\pi n_s e^2)/m^* c(n_0 + n_{Si})$, $\omega_c = eB/m^*c$, n_0 and n_{Si} are the indices of refraction for the oxide and Si respectively, and n_s is the surface electron density. In the second case, the Si-air interface is assumed to be parallel to the Si-SiO_2 interface and separated by a distance d. The resulting transmission is[17]

$$T = 2n_0 n_a X^-\{\cos^2\theta[(n_a+n_0)^2X^- + (2n_a+2n_0+\Omega)\Omega] + n_{Si}^{-2}\sin^2\theta[(n_0n_a+n_{Si}^2)^2X^- + (2n_0n_a+2n_{Si}^2+n_a\Omega)n_a\Omega]$$
$$-n_{Si}^{-1}\cos\theta\sin\theta[(n_a+n_0-n_an_0+n_{Si}^2)2\Omega(\omega-\omega_c)\tau]\}^{-1} + 2n_0^2X^+\{X^- \to X^+; -\omega_c \to \omega_c\}^{-1}, \quad (2)$$

where $\Omega = 4\pi n_s e^2\tau/m^*c$, n_a is the index of refraction of air, $\theta = (n_{Si}\omega/c)d$, and the other symbols are as defined for Eq. (1). Here the transmission has *not* been normalized by the gate-off, $n_s = 0$, result. Equation (2) has been helpful in dealing with residual interference effects; however, when applied to a situation in which the wedging has effectively eliminated interference affects, Eq. (2) with $\theta = 0$ overestimates the absorption line intensity at high electron densities (typically $n_s \approx 10^{12}$ cm^{-2}). This is due to the added absorption in the 2DEG during successive radiation transits through the Fabry-Perot structure. Thus forcing a fit to Eq. (2) for high density data on a properly wedged sample requires a much longer τ for the (over-absorbed) calculated line shape than would be determined from the single-pass expression [Eq. (1)]. However, for $\theta = 0$ (or 90°), the line *shape* and peak *position* calculated from the multiple-pass expression are the same as for the single-surface expression.

It will be shown later that a magnetic-field-dependent τ is required under some experimental conditions as predicted by Ando[18] (usually at $n_s \gtrsim 10^{12}$ cm^{-2} and $\tilde{\nu} > 25$ cm^{-1}). In such cases, $\tau(B) \propto B^{-1/2}$ simply replaces τ in Eqs. (1) or (2). A justification for using this scattering time will be presented in the discussion of results. The use of $\tau(B)$ produced a better fit to the data than could be achieved with a constant τ_0. The results for the mass obtained in this way are systematically only about 1% higher than those obtained with constant τ_0 fits and there is no difference in the scattering time obtained; i.e., $\tau(B_c) = \tau_0$, where B_c is the field at resonance.

A. Frequency and density dependence of the CR parameters

While extensive measurements have been made on each of the four samples of Fig. 3, presentation of m^* and τ for samples 2 and 3, Figs. 6–9, are sufficient to display the main qualitative features observed in these experiments. At each frequency and for each sample (except sample 1 at 11.2 cm^{-1} and sample 3 at 5.8 cm^{-1}) the effective mass shows a maximum as a function of electron density. This maximum occurs at progressively lower densities as the laser frequency or resonant magnetic field is decreased. With the exception of sample 3 at $\tilde{\nu} = 61.3$ cm^{-1}, at any selected metallic density (roughly $n_s \gtrsim 5\times10^{11}$ cm^{-2}), the effective mass increases as the laser frequency or magnetic field decreases. This result has been obtained for all samples investigated. Thus it does not appear that the frequency dependence of the mass is sample dependent. The observed frequency-dependent mass contrasts with the results reported by Abstreiter *et al.*[6] where only a very small systematic frequency dependence (less than the experimental error) was observed over a range of frequencies between 3 and 30 cm^{-1}. This point is discussed further in the following section. For all cases in the metallic density region, the effective mass is greater than (or enhanced over)

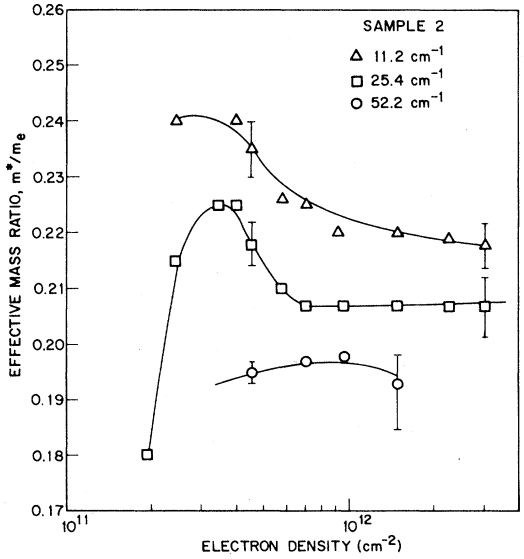

FIG. 6. Variation of effective mass with electron density at several laser frequencies for sample 3 at $T = 4.5$ K. Representative error bars are indicated.

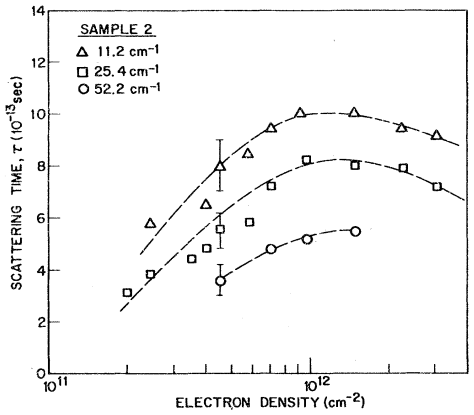

FIG. 7. Variation of scattering time with electron density at several laser frequencies for sample 2 at $T = 4.5$ K. Representative error bars are indicated.

the transverse effective mass of the bulk Si (100) ellipsoids of $m_0^* = 0.1915 m_e$.[21]

Over most of the region studied, the density dependence of the scattering time is qualitatively similar to that of τ determined from the effective mobility ($\mu = e\tau/m^*$), albeit with some overall reduction as the frequency or magnetic field is increased.

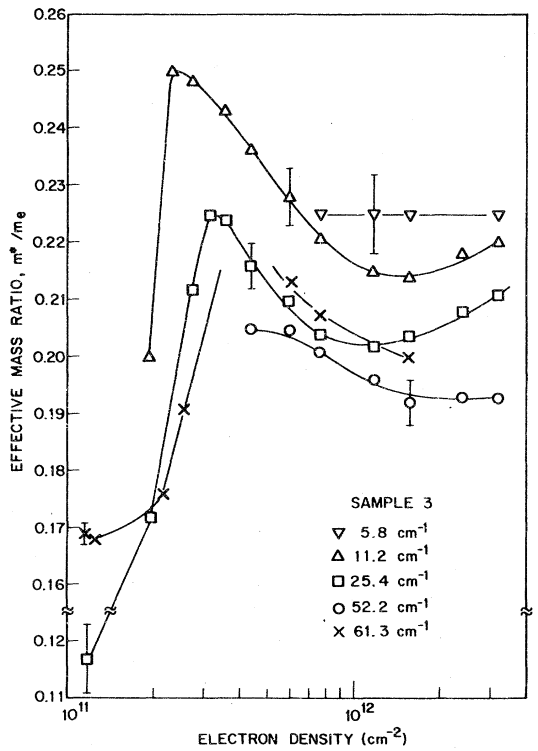

FIG. 8. Variation of effective mass with electron density at several laser frequencies for sample 3 at $T = 4.5$ K. Error bars at several representative points are shown.

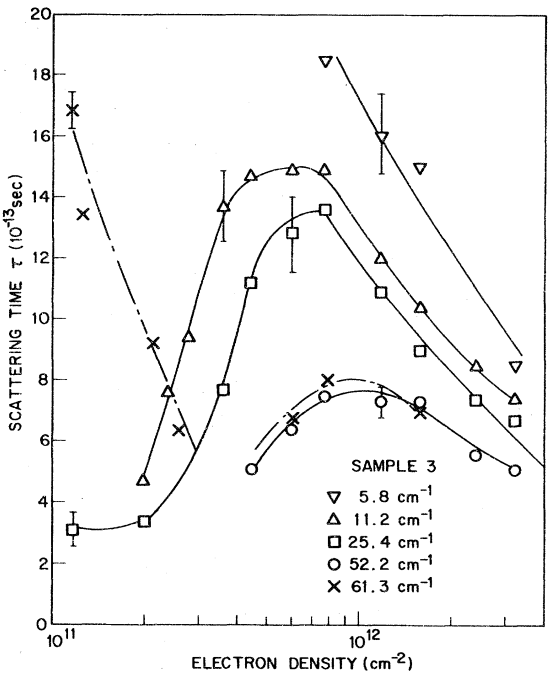

FIG. 9. Variation of scattering time with electron density at several laser frequencies for sample 3 at $T = 4.5$ K. Representative error bars are indicated.

It should be emphasized that a clearly defined resonant absorption line is observed at densities for which the dc conductivity is thermally activated. In this region, however, the effective mass and scattering time exhibit very complicated behavior. In general, the effective mass goes through a peak and then a strong reduction as density is decreased below $(2-6)\times10^{11}$ cm^{-2} (depending on frequency or magnetic field). This is shown clearly in Fig. 8. For the highest mobility samples and at the highest frequency, the mass reduction is accompanied by an order-of-magnitude *increase* in scattering time (Fig. 9).

B. Temperature dependence

The temperature dependences of the resonance parameters of sample 3 for $\bar{\nu} = 25.4$ cm^{-1} are shown in Figs. 10 and 11. At the highest density studied, $n_s = 1.59\times10^{12}$ cm^{-2}, the effective mass and scattering time are nearly constant within experimental error over the temperature range 1.5–35 K. At the other density extreme, $n_s = 1.15\times10^{11}$ cm^{-2}, both the effective mass and scattering time increase with temperature. The data at intermediate densities, particularly at $n_s = 3.2\times10^{11}$ cm^{-2}, where the mass is significantly enhanced over m_0^* at low temperatures, exhibit qualitatively different behavior from either the low- or high-density regimes. For example, at $n_s = 3.2\times10^{11}$ cm^{-2}, the mass *decreases* substantially, ap-

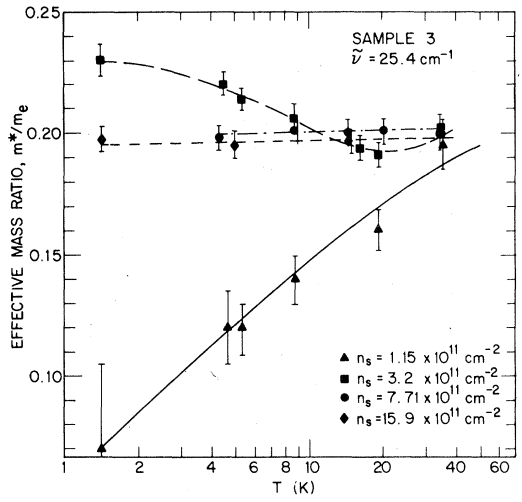

FIG. 10. Variation of effective mass with temperature at several electron densities for sample 3 and $\tilde{\nu} = 25.4$ cm^{-1}.

proaching m_0^* as the temperature is increased, while the scattering time decreases. These data clearly demonstrate the qualitatively different behaviors that occur in the different density regions. As a result, attempts at interpretation must distinguish physically among these different regions.

C. Effect of interband light

As was mentioned in Sec. II, the character of the depletion layer may affect the CR parameters. To test this possibility, sample 3 was illuminated with an *in situ* 600-nm light-emitting diode (LED). This has the effect of creating a large number of electron-hole pairs in the Si near the interface. In the depletion layer these carriers neutralize the fixed depletion charge on the one hand while increasing the inversion-layer density above the equilibrium density for the given gate voltage on the other hand. This creates a steady-state quasi-accumulation situation in which the fixed depletion charge is very small. As shown in Fig. 12, a substantial increase in the resonance absorption is observed when the LED is on for the lower gate voltage data. This demonstrates that, for fixed gate voltage, the LED radiation increases the inversion-layer electron population as expected. This same effect can be seen in the shift with LED radiation of the high-field (6–7 T and 8–9 T)

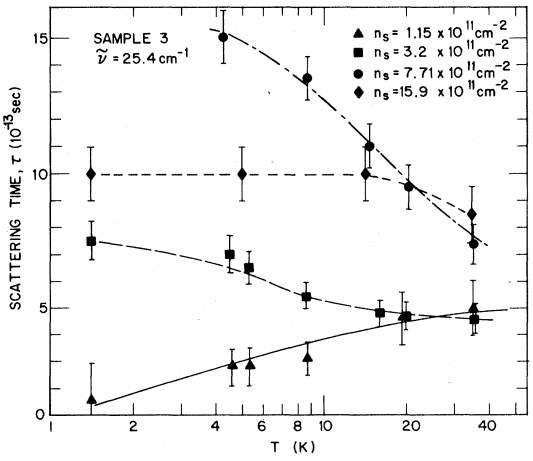

FIG. 11. Variation of scattering time with temperature at several electron densities for sample 3 and $\tilde{\nu} = 25.4$ cm^{-1}.

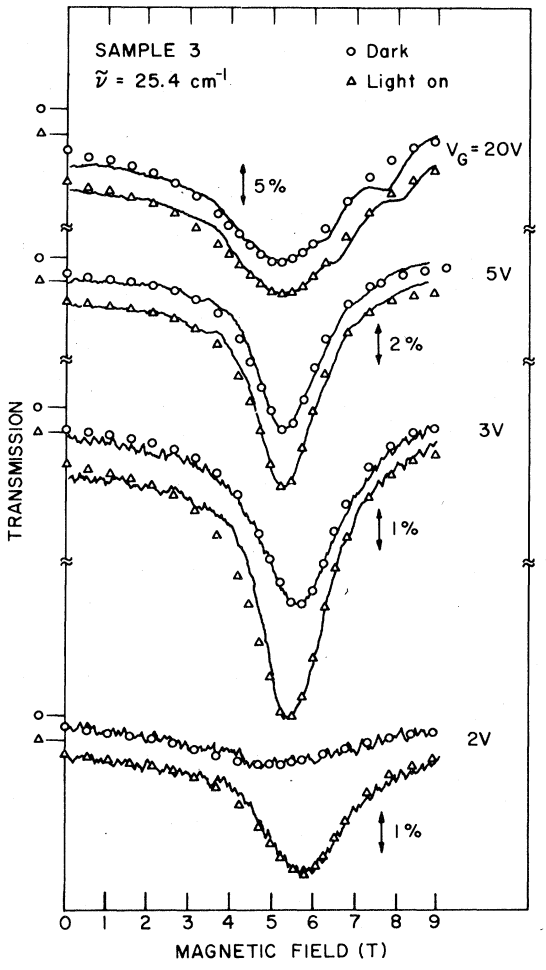

FIG. 12. Cyclotron-resonance transmission for sample 3 at $\tilde{\nu} = 25.4$ cm^{-1}. "Dark" refers to the normal operating conditions as described in the text. "Light on" refers to the case where the sample was illuminated with 600-nm LED radiation. The *calculated* results for these two conditions are shown by O and Δ, respectively. The 100% points are shown outside the left margin of the figure. The two cases are slightly displaced for clarity of presentation. The fitting parameters are presented in Figs. 13 and 14.

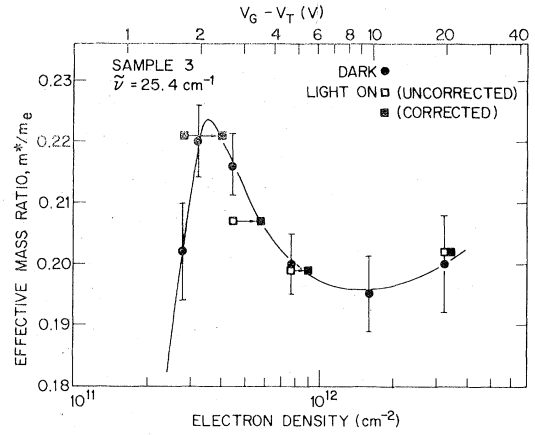

FIG. 13. Variation of effective mass with electron density for sample 3, $\tilde{\nu}$ = 25.4 cm^{-1}, T = 4.5 K with LED radiation off (●) and on (□). When density is corrected as described in the text, the "corrected" data points (■) result.

quantum oscillations for $V_G = 20$ V which is also indicative of an increased electron population (larger Fermi energy). By identifying the Landau level associated with each oscillation, noting the shift in magnetic field, and relating this to n_s by recourse to magnetotransport results, an estimate of the change of n_s can be made. The value thus determined ($\Delta n_s \simeq 1.5 \times 10^{11}$ cm^{-2}) is equal to the value of the equilibrium depletion charge in strong inversion within experimental error. Thus it is clear that the LED radiation at the power levels used reduces strongly (or completely eliminates) the depletion layer.

The CR parameters based on the above observations are plotted onto a corrected density scale,

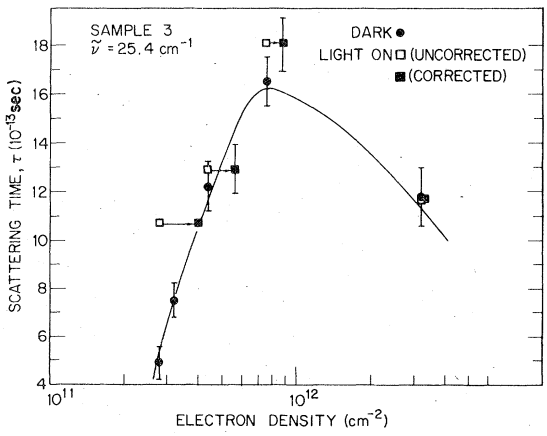

FIG. 14. Variation of scattering time with electron density for sample 3, $\tilde{\nu}$ = 25.4 cm^{-1}, T = 4.5 K, with LED radiation off (●) and on (□). When the density is adjusted as described in the text, the "corrected" data points (■) result.

n_s (LED on) = n_s (LED off) + 1.5×10^{11} cm^{-2}, in Figs. 13 and 14. Within experimental uncertainty, the change in CR parameters are entirely accounted for by the increase in inversion-layer density. Thus, by implication, the CR parameters do not depend on depletion layer charge density (and hence on the subband separation) at this temperature.

IV. DISCUSSION OF RESULTS

A. High electron density

While these experiments yield a more precise measure of effective mass than of scattering time, it is preferable to discuss the dependence on scattering time first in order to make contact with theoretical results.

At $n_s = 1 \times 10^{12}$ cm^{-2}, the electron Fermi energy is 6 meV, considerably larger than kT for all the data reported here. Thus, the electron system at densities greater than 10^{12} cm^{-2} can be described as a degenerate, two-dimensional electron Fermi gas, since localization effects do not persist to this density. The application of a strong magnetic field results in the complete quantization of the electron gas. Ando[18] has calculated the high-frequency conductivity for a noninteracting electron gas in a self-consistent Born approximation. In the high-field ($\omega_c \tau \gg 1$) region, short-range scattering [$b \ll l$, where b is the range of the scattering potential and $l = (c\hbar/eB)^{1/2}$ is the cyclotron radius] limit, the theory predicts that $1/\tau \propto B^{1/2}$. More recent calculations have confirmed this limiting behavior.[19,20]

As has been stated earlier, some of the present data has been fitted with this field-dependent scattering rate. The principal reason for using $\tau(B)$ is the general improvement in the overall fit to the high-frequency data at metallic densities when $\omega_c \tau \gg 1$. A compilation of the scattering rate obtained at the various resonant magnetic fields is shown in Fig. 15. The experimental uncertainty makes it difficult to make a precise statement regarding the magnetic field dependence of the scattering rate. However, it is clear that the data are *consistent* with a scattering rate increasing with magnetic field as $B^{1/2}$ at the highest fields. This supports the use of a field-dependent rate to fit the experimental data in the high $\omega_c \tau$, high n_s regime (where the metallic electrons are effective in screening the charged scattering centers leading to effective short-range scattering). On the other hand, at the lower fields (lower values of $\omega_c \tau$) the dependence of scattering rate on field is somewhat weaker.

Figures 6 and 8 show strong variations of m^*

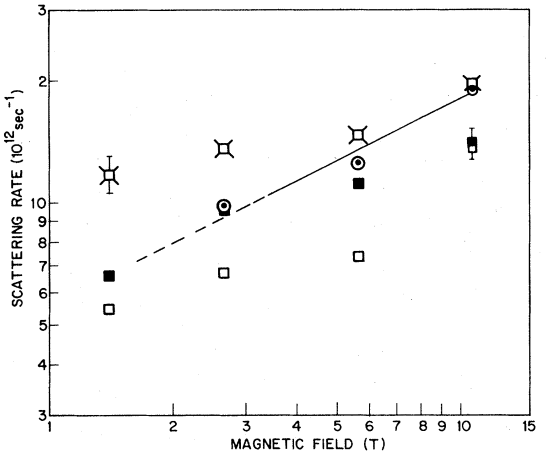

FIG. 15. log-log plot of the scattering rate versus magnetic field for various samples and electron densities. Sample 3, ⌑ for $n_s = 3.23 \times 10^{12}$ cm^{-2}, ■ for $n_s = 1.59 \times 10^{12}$ cm^{-2}, □ for $n_s = 7.71 \times 10^{11}$ cm^{-2}; sample 2, ○ for $n_s = 1.49 \times 10^{12}$ cm^{-2}, ● for $n_s = 9.71 \times 10^{11}$ cm^{-2}. The sample temperature was 4.5 K. The straight line has a slope of $\frac{1}{2}$.

with n_s and frequency in the metallic density region. In preliminary work,[4] it has been argued that the frequency or magnetic field variation of the effective mass in this density regime correlates with the variation of $\omega\tau$. In order to examine this point of view further, both the ω and $\omega\tau$ dependence of m^* are presented in Fig. 16 for all four samples at selected electron densities.

The data of Fig. 16(a) shows that for samples 2, 3, and 4, m^* decreases toward the bulk effective mass as frequency is increased. In the case of sample 1, this correlation is not clear, since the mass value at $n_s = 1.59 \times 10^{12}$ cm^{-2} and $\tilde{\nu} = 11.2$ cm^{-1} appears to be too low. It should be noted that this is the lowest mobility sample and the mobility is still increasing as n_s is increasing toward 1.5×10^{12} cm^{-2} (see Fig. 3). Thus, by comparison with the other samples it is likely that the effective mass still reflects a residual "low-density" mass reduction, as discussed below. The straight line in Fig. 16(a) represents a least-squares fit to all of the data points with a correlation coefficient $r = 0.779$ ($r = 1$ when all points are on a straight line). Thus it appears that all of the samples show a qualitatively similar frequency dependence of the mass. However, the magnitude of the mass enhancements at a given frequency depend on the sample. In an attempt to understand the sample-to-sample variation, the effective mass vs $\omega\tau$ has been plotted in Fig. 16(b). In this way, sample-to-sample differences are included in a rough way through the cyclotron-resonance scattering time τ. Figure 16(b) shows that there is correlated

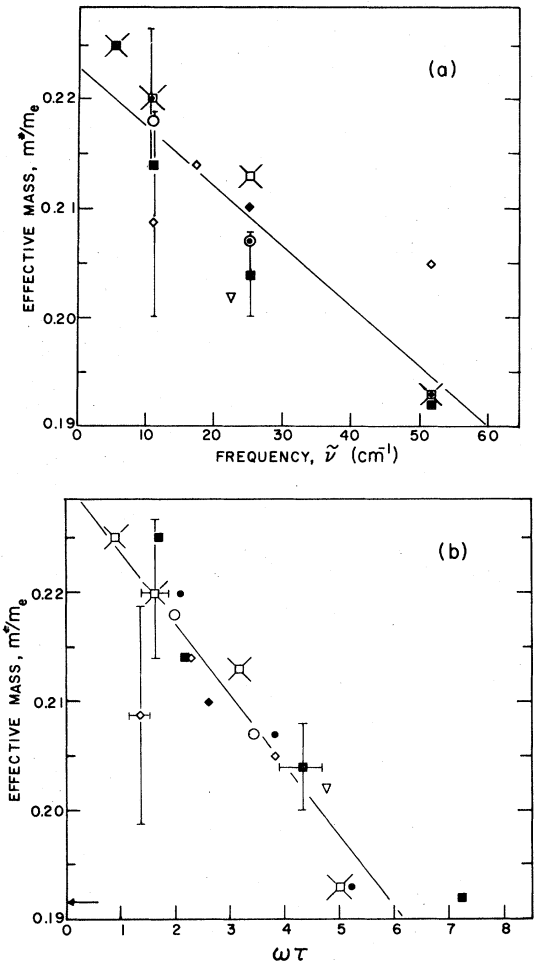

FIG. 16. Plots of cyclotron effective mass determined from classical fits to the absorption lines versus (a) laser frequency and (b) $\omega\tau$, where τ is the scattering time determined from the fit. The symbols have the following correspondences: ◇ and ♦—sample 1 for $n_s = 1.4 \times 10^{12}$ and 2.4×10^{12} cm^{-4}, respectively; ● and ○—sample 2 for $n_s = 1.49 \times 10^{12}$ and 3.04×10^{12} cm^{-2}, respectively; ■ and ⌑—sample 3 for $n_s = 1.59 \times 10^{12}$ and 3.23×10^{12} cm^{-2}, respectively; and ▽—sample 4 for $n_s = 1.07 \times 10^{12}$ cm^{-2}. The straight lines in (a) and (b) represent linear least-squares fits to the data.

behavior when the data are plotted in this fashion. Here the least-squares fitted straight line has a correlation coefficient of $r = 0.816$. This represents an excellent fit to the data in light of the problems with sample 1, the additional data scatter introduced by τ, and since it is not anticipated that the mass enhancement would approach the bulk value in a strictly linear fashion. In addition, it is noteworthy that for sample 3, this correlation is supported by the upturn in mass with density (see Fig. 8) at 11.2 and 25.4 cm^{-1} as scattering time (see Fig. 9) decreases.

As mentioned previously, experimental results

of Abstreiter *et al.*[6] appear to be in disagreement with the present data. It is not completely clear what the cause of the discrepancy is; however, our studies of samples with different processing conditions seem to indicate that it is not due to sample differences. Apart from sample considerations, there are a number of other differences in experimental conditions between laboratories which might account for the differences in cyclotron-resonance parameters. The care that we have taken to eliminate coherent interference and multiple internal reflection effects (both of which can distort line shapes and give systematic errors in effective masses[17]), as well as the internal consistency of the results on a number of samples, gives us confidence in these results.

A preliminary report[4] of the correlations which are confirmed in Fig. 16 was the basis for invoking electron-electron interactions to explain the observed mass enhancement. The dimensionless parameter r_s (the ratio of the average kinetic energy to the average Coulomb energy per particle) is generally used as a measure of how "metallic" or dense an electron gas is in terms of electron-electron interactions. For a two-dimensional electron gas $r_s^2 = 1/n_s a_0^2$, where $a_0 = \kappa\hbar^2/m_0^* e^2$ is the effective Bohr radius with κ the dielectric constant and m_0^* the band effective mass. Several years ago Smith and Stiles[22] carried out a series of measurements of the effective mass of electrons in Si (001) inversion layers as determined from the temperature dependence of the amplitude of Shubnikov–de Haas oscillations. A variation of the observed mass with density (r_s ranged between 0.9 and 2.1) was interpreted in terms of electron-electron enhancement of the quasiparticle mass. Although the experimental results appear to be sample dependent,[10] several theoretical calculations[23,24] have since lent additional credence to this interpretation. In addition, optical experiments[25] which probe quantized energy levels perpendicular to the surface (the electric subband separations), as well as theoretical calculations,[26] have demonstrated that electron-electron interactions can play an important role in determining the electronic subband energies. Thus, it is natural to consider whether mass enhancement effects can be observed in the high-frequency conductivity parallel to the surface (interface) through a cyclotron-resonance experiment.

Theoretical arguments by Kohn[27] and others would seem to preclude the observation of electron-electron interactions in such an experiment. The results of Kohn's proof can be stated as follows: For a translationally invariant system of free electrons in the presence of a uniform external magnetic field and a uniform high-frequency electromagnetic field with electron-electron interactions taken into account, the *only* electric dipole allowed transition is cyclotron resonance which occurs at an angular frequency $\omega_c = eB/m_0^* c$, where m_0^* is the electron effective mass undressed by electron-electron interactions. Thus any additional electric dipole transitions which are observed for electrons in a solid must arise from: (1) band structure effects in the solid, (2) nonuniformity of the incident electromagnetic fields, which are used to probe the system, (3) breaking of the translational invariance due to, e.g., a fixed random array of scattering centers which could exist in the solid, or (4) interactions with other elementary excitations of the solid, such as phonons. Any one or a combination of these effects can also remove the condition that cyclotron resonance must occur at a frequency (magnetic field) determined by the undressed electron mass. In particular, it is easy to show[28] that the inclusion in the Hamiltonian of an interaction potential between the electrons and a random array of fixed charge centers of the form $\sum_{i,j} V_{ij}(R_i - r_j)$, where R_i is the position of the ith fixed charge center and r_j is the jth electron coordinate, leads to a coupling of the center of mass and relative degrees of freedom of the electron gas. In the absence of these fixed charge centers (for electrons with a parabolic dispersion relation) the center of mass and relative coordinates are separable, and an external uniform high-frequency electric field couples *only* to the center-of-mass degrees of freedom. Since the electron-electron interactions are contained only in the *relative* degrees of freedom, this is a statement of the physics underlying Kohn's proof. Thus it is clear that under the proper circumstances, electron-electron effects might be observed in a cyclotron-resonance (high-frequency) experiment.

It has been argued previously that, in the present experiment, translational invariance is broken by the presence of a random array of scattering centers at or near the $Si\text{-}SiO_2$ interface thus allowing apparent mass enhancement due to electron-electron interactions to be observed. A qualitative measure of the importance of these scattering centers in the CR experiment is the value of $1/\omega\tau$. Based on these considerations it is expected that as $\omega\tau$ increases, any apparent mass enhancement in the CR experiment would be reduced. Following this suggestion, a number of theoretical treatments were presented. Ando,[29] using an approximation akin to Fermi-liquid theory, has shown how the cyclotron-resonance harmonics appear and exhibit mass enhancement. His theory predicts a very small shift for the funda-

mental cyclotron resonance. Ting *et al.*[30] have calculated the frequency-dependent conductivity of an interacting gas in the presence of a random array of scattering centers and a dc magnetic field using a memory-function approach. Their results indicate a frequency-dependent mass. Quantitative comparisons[31] require numerous approximations; the results yield frequency dependence less than that observed. Tzoar *et al.*[32] and later Ganguly and Ting[33] have calculated the frequency-dependent conductivity at zero magnetic field. Tzoar *et al.* obtain a frequency- and density-dependent mass shift, $\Delta m = m^* - m_0^*$, given by

$$\frac{\Delta m}{m_0^*} = \frac{r_s}{\sqrt{2}} \left(\frac{n_I}{n_s}\right) N(\bar{\Omega}, r_s) , \tag{3}$$

where $\bar{\Omega} = \hbar\omega/4E_F$, $N(\bar{\Omega}, r_s)$ is an integral function which is evaluated numerically, and n_I is the two-dimensional density of scattering center; $N(\bar{\Omega}, r_s)$ decreases rather strongly with frequency at constant density. For a Coulomb scattering potential the theory of Ting *et al.*[30] yields identical results in the limit of $B = 0$.[31]

The experimental data of sample 3 have been replotted in Fig. 17 in the region of metallic densities in such a way that they can be compared with the predictions of Eq. (3). A quantity $\Delta m / m_0^* N(\bar{\Omega}, r_s)$ is plotted vs $n_s^{-3/2}$, where $\Delta m = m^* - 0.191 m_e$, with m^* the experimentally determined effective mass and $N(\bar{\Omega}, r_s)$ obtained from Fig. 1 of Ref. 32; $\bar{\Omega}$ is determined from the laser frequencies and measured densities. All the data fall on straight lines with a common slope over a significant range of densities as expected from Eq. (3). Ganguly and Ting[33] have extended the work of Tzoar *et al.* to take into account the finite thickness of the inversion layer and the twofold valley degeneracy. They conclude that their

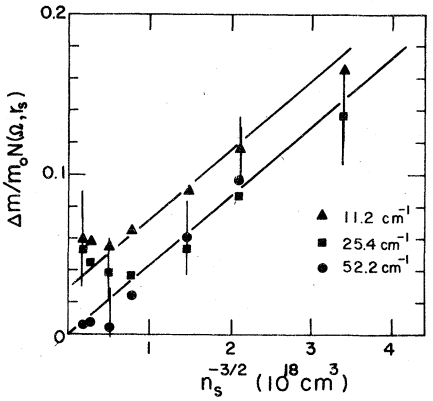

FIG. 17. A plot of the effective-mass shift for sample 3 as a function of $n_s^{-3/2}$ for three laser frequencies (ν = 11.2, 25.4, and 52.2 cm^{-1}, respectively) and T = 4.5 K.

numerical results show qualitative agreement with experiment.

It should be noted that there also appears to be qualitative agreement with Ganguly and Ting in connection with the temperature dependence of the effective mass. While the data is not extensive, Figs. 10 and 11 show that the effective mass and scattering time at the highest density have little temperature dependence. As the density is reduced to 3.2×10^{11} cm^{-2}, the strong mass enhancement is reduced as temperature is increased. Similarly, down to $n_s = 3.2 \times 10^{11}$ cm^{-2}, the scattering time is reduced as temperature is increased. In both cases, this is the dependence suggested by Ganguly and Ting. This generally good qualitative agreement down to such low densities may be fortuitous, however. Transport results at zero magnetic field indicate that thermally activated behavior is to be expected below $n_s \approx 5 \times 10^{11}$ cm^{-2}. In this density region, it may be inappropriate to apply a theoretical formalism which assumes an interacting *metallic* electron gas. On the other hand, it should be noted that the mass enhancement at $\tilde{\nu} = 11.2$ cm^{-1} persists to densities well into the thermally activated region. In order to explain this result, it might be postulated that the magnetic field causes a downward shift of the density for the boundary between activated and metallic conductivity. It would then be reasonable to expect the thermally activated region to shift to even lower densities with further increase of magnetic field or laser frequency with a concomitant shift of the region of enhancement to lower densities at the high laser frequencies, precisely opposite to observation.

The possibility that the metallic density mass enhancement is due to either population of the fourfold degenerate higher subbands (heavy-mass valleys) of Fig. 2(b) or coupling between the fourfold and twofold valleys must also be considered. Effective mass enhancement under quasiaccumulation conditions at high temperatures and low densities[7] and under uniaxial stress[8,9] has been explained by invoking such effects. For the metallic density results of the present experiment, cyclotron-resonance absorption spectra taken with T up to 35 K showed no evidence that the heavy-mass valleys were populated, i.e., no heavy-mass resonance was observed. Furthermore, the effective-mass variations with T for $n_s = 1.59 \times 10^{-12}$ and 7.71×10^{11} cm^{-2} (Fig. 10) do not show any unusual behavior; the mass is essentially independent of temperature. Finally, the proposed coupling of light- and heavy-mass valleys seems unlikely based on the results of the band-gap radiation experiments. Since light modifies the surface potential drastically by neutralizing the

depletion charge, the coupling to higher subbands should also change substantially. Thus the light should modify the mass (increase it) if the enhancement were due to coupling to higher subbands. Since no such effect is observed, this possibility cannot be responsible for the metallic density mass enhancement.

B. Low densities

At electron densities below 5×10^{11} cm^{-2}, all samples used in this study exhibit thermally activated conductivity at zero magnetic field. This behavior has usually been explained in terms of the Mott-Anderson localization due to static potential fluctuations at the Si-SiO_2 interface. Since well-defined cyclotron-resonance spectra are observed in this density region, it is necessary to examine these data, bearing in mind the fact that the electrons may be in localized states substantially different from the continuum states that characterize the metallic density regime.

The data of the first cyclotron-resonance experiment in this low-density region[3] were analyzed in terms of noninteracting electrons localized in static harmonic-oscillator potential wells.[34] Although a carefully selected set of harmonic potentials and ranges was required, this model did yield qualitative agreement with experiment, namely a cyclotron mass reduction to values well below the bulk mass at the lowest densities, $n_s\approx3\times10^{11}$ cm^{-2}.

The present data pose a number of problems for this model. Firstly, an *enhanced* mass is observed well into the localized density regime. Secondly, down to $n_s\approx2\times10^{11}$ cm^{-2}, the ordering of effective mass with magnetic field or laser frequency is contrary to the predictions of the model, i.e., as the laser frequency is increased, the effective mass should increase at constant density. Thus it appears that the model is inappropriate for data at $2\times10^{11}\lesssim n_s\lesssim5\times10^{11}$ cm^{-2}. (Further comments on this model as it applies to the very lowest density region are given below.)

It should be reemphasized that the density region where the effective mass is changing rapidly and peaks (depending on the frequency of observation, $n_s=2$–4×10^{11} cm^{-2}) appears to be a region of physical behavior qualitatively different than either the high- or low-density regimes. As such, it may represent a region of very complicated behavior in which both low- and high-density phenomena are involved. However, some insight into the problem can be obtained by noting that the mass peak occurs approximately when the cyclotron orbit radius l is equal to the average electron separation, $r_0=(\pi n_s)^{-1/2}$. Furthermore, it should be noted that even though samples 2 and 3 have substantially different transport properties, the magnitude of the peak mass enhancement and the density at which the peak occurs agree within experimental uncertainty. These observations suggest that even at electron densities where transport shows localized behavior, electron-electron interactions are playing a dominant role in the cyclotron-resonance measurement. In this regard, it has been shown[35,36] that local structural deformations (Si lattice relaxation) at the Si-SiO_2 interface can mediate a substantial electron-electron interaction. Such an effect could produce the observed mass enhancement.

The only data presented here which show the lowest density behavior are those taken on sample 3 at $n_s=(1$–$2)\times10^{11}$ cm^{-2} (Figs. 8 and 9). However, extensive measurements on sample 4 have recently been made at $\tilde{\nu}=19.5$–61.3 cm^{-1}, $n_s=6\times10^{9}$–5×10^{11} cm^{-2}, and $T=1.5$–4.5 K.[37] These results, and results obtained at fixed B while varying $\tilde{\nu}$,[38] corroborate the behavior of m^* and τ shown in Figs. 8 and 9. That is, in the region where $r_0\gtrsim2l$ (i.e., the lowest Landau level is less than half filled) a line sharpening is observed. In Fig. 9, τ increases to greater than 10^{-12} sec. In this region, the effective mass is less than the bulk effective mass. From data taken on sample 4, it can be shown that this shifted effective mass behaves like an "impurity-shifted" cyclotron resonance[37] with an energy intercept extrapolated to zero magnetic field of 10 cm^{-1} and a slope of 4.4 cm$^{-1}/T$. To some extent, this behavior is compatible with the model of cyclotron resonance of electrons localized in harmonic-oscillator potential wells.[34] However, two difficulties present themselves: (1) Since the absorption line is very sharp, a very unique set of harmonic-oscillator wells would be required and (2) the model predicts no dependence on the degree of Landau-level filling, whereas the data show a clear correlation with this parameter. Since the results for sample 4 are quite complicated and do not contribute materially to the main topic of this paper, the reader is referred to Refs. 5 and 37 for a more extensive presentation and discussion of the data.

V. CONCLUSION

The cyclotron-resonance experiments reported here on a set of Si (001) MOSFET's have yielded a consistent set of experimental parameters. In the high limit of frequency, density, and temperature, the effective mass agrees well with the bulk Si (001) effective mass. As a result, it is concluded that the experiments are not affected by a systematic error(s).

In the high electron density regime, the behavior

of scattering time with magnetic field ($1/\tau \propto B^{1/2}$) shows the importance of electron–short-range-potential scattering processes. In the case of the effective-mass variation at high density, there is strong evidence for a correlation of m^* with both ω and $\omega\tau$. While some theoretical calculations based on the role of electron-electron interactions predict this behavior, only qualitative agreement has as yet been achieved. Certainly it is premature to exclude other theoretical models from consideration.

It must be reemphasized that the evidence for a frequency-dependent effective mass does not appear to be corroborated in the other experimental study. This disagreement may hinge on details as to sample characteristics, experimental environment, fitting procedure, and estimation of random experimental errors. At present however, no basis exists to reconcile the two experiments.

The role of background illumination has been shown to produce a very straightforward trade-off of depletion charge (inversion case) for mobile charge (quasiaccumulation case). As a result, this difference in experimental environment does not appear to be responsible for experimental disagreements at low temperature (near 4.5 K). Whether or not more subtle effects are present under background illumination has not been determined.

At low densities, the variation of m^* and τ have a unique and complicated behavior. While the evidence appears to be fairly strong that collective, electron-electron effects are important in this density region, this case will not be argued here. Rather the reader is referred to more extended discussions elsewhere.[5,37,38]

ACKNOWLEDGMENTS

The authors wish to acknowledge very useful conversations with K. L. Ngai, T.L. Reinecke, J. J. Quinn, and C. T. White, and the technical support of G. Kaminsky and the staff of the NRL High Magnet Field Facility.

[1]G. Abstreiter, P. Kneschaurek, J. P. Kotthaus, and J. F. Koch, Phys. Rev. Lett. 32, 104 (1974); and S. J. Allen, D. C. Tsui, and J. V. Dalton, *ibid.* 32, 107 (1974).

[2]See, for example, Proceedings of the Second International Conference on the Electronic Properties of 2*D* Systems, Berchtesgaden, 1977 [Surf. Sci. 73, 1–564 (1978)]. A review of magneto-optical studies is included, J. P. Kotthaus, Surf. Sci. 73, 472 (1978).

[3]J. P. Kotthaus, G. Abstreiter, J. F. Koch, and R. Ranvaud, Phys. Rev. Lett. 34, 151 (1975); G. Abstreiter, J. P. Kotthaus, J. F. Koch, and G. Dorda, Phys. Rev. B 14, 2480 (1976).

[4]T. A. Kennedy, R. J. Wagner, B. D. McCombe, and D. C. Tsui, Phys. Rev. Lett. 35, 1031 (1975).

[5]T. A. Kennedy, R. J. Wagner, B. D. McCombe, and D. C. Tsui, Solid State Commun. 21, 459 (1977).

[6]G. Abstreiter, J. F. Koch, P. Goy, and Y. Couder, Phys. Rev. B 14, 2494 (1976).

[7]H. Kühlbeck and J. P. Kotthaus, Phys. Rev. Lett. 35, 1019 (1975).

[8]P. Stallhofer, J. P. Kotthaus, and J. F. Koch, Solid State Commun. 20, 519 (1976).

[9]P. Stallhofer, J. P. Kotthaus, and G. Abstreiter (unpublished).

[10]F. F. Fang, A. B. Fowler, and A. Hartstein, Surf. Sci. 73, 269 (1978); Phys. Rev. B 16, 4446 (1977).

[11]R. J. Wagner, A. J. Zelano, and L. H. Ngai, Opt. Commun. 8, 46 (1973).

[12]A. Kamgar, D. C. Tsui, and M. D. Sturge, Solid State Commun. 24, 47 (1977).

[13]C. C. Hu, J. Pearse, K. M. Cham, and R. G. Wheeler, Surf. Sci. 73, 207 (1978).

[14]F. Neppl. J. P. Kotthaus, J. F. Koch, and Y. Shiraki, Phys. Rev. B 16, 1519 (1977).

[15]S. M. Sze, *Physics of Semiconductor Devices* (Wiley-Interscience, New York, 1969), p. 436.

[16]M. von Ortenberg, Solid State Commun. 17, 1335 (1975).

[17]T. A. Kennedy, R. J. Wagner, B. D. McCombe, and J. J. Quinn, Solid State Commun. 18, 275 (1976).

[18]T. Ando, J. Phys. Soc. Jpn. 38, 989 (1975).

[19]S. Fujita and M. Prasad, J. Phys. Chem. Solids 38, 1351 (1977); M. Prasad and S. Fujita, Solid State Commun. 23, 551 (1977).

[20]W. Götze and J. Hajdu, Solid State Commun. 29, 89 (1979).

[21]J. C. Hensel, H. Hasagawa, and M. Nakayama, Phys. Rev. 138, A225 (1965).

[22]J. L. Smith and P. J. Stiles, Phys. Rev. Lett. 29, 102 (1972).

[23]C. S. Ting, T. K. Lee, and J. J. Quinn, Phys. Rev. Lett. 34, 870 (1975); T. K. Lee, C. S. Ting, and J. J. Quinn, Solid State Commun. 16, 1809 (1975).

[24]B. Vinter, Phys. Rev. Lett. 35, 1044 (1975).

[25]P. Kneschaurek and J. F. Koch, Phys. Rev. B 16, 1590 (1977), and references therein.

[26]T. Ando, Surf. Sci. 73, 1 (1978), and references therein.

[27]W. Kohn, Phys. Rev. 123, 1242 (1961).

[28]See, e.g., J. J. Quinn, B. D. McCombe, K. L. Ngai, and T. L. Reinecke, Phys. Lett. 54A, 161 (1975).

[29]T. Ando, Phys. Rev. Lett. 36, 1383 (1976).

[30]C. S. Ting, S. C. Ying, and J. J. Quinn, Phys. Rev. Lett. 37, 215 (1976).

[31]J. J. Quinn (private communication).

[32]N. Tzoar, P. M. Platzman, and A. Simons, Phys. Rev. Lett. 36, 1200 (1976).
[33]A. K. Ganguly and C. S. Ting, Phys. Rev. B 16, 3541 (1977).
[34]H. J. Mikeska and H. Schmidt, Z. Physik B 20, 43 (1975).
[35]K. L. Ngai and T. L. Reinecke, Phys. Rev. Lett. 37, 1418 (1976).
[36]K. L. Ngai and C. T. White, Surf. Sci. 73, 31 (1978); and Surf. Sci. (in press).
[37]R. J. Wagner and D. C. Tsui, J. of Magn. Magn. Mater. 11, 26 (1979); Surf. Sci. (in press).
[38]B. A. Wilson, S. J. Allen, Jr., and D. C. Tsui, Phys. Rev. Lett. 44, 479 (1980); Surf. Sci. (in press).